A Paleomagnetic Exploration of the Sierra Madre Oriental

Emily R. Schottenfels

Honors Thesis

Earth and Environmental Sciences

Acknowledgment

First off, I would like to express my deepest appreciation and gratitude to my advisor, Dr. Rob Van der Voo. It has been both an honor and a privilege to learn and work with him over the two years. I have learned a tremendous amount from this experience that goes beyond the topic of paleomagnetism. I am forever grateful for his continuous guidance and encouragement.

This thesis could not be a reality without the help from PhD Candidate, Samantha Nemkin. I am incredibly appreciative for the hours spent teaching me how to use the instruments, computer programs, and always providing help (especially during the darkest times of the project). Her availability and willingness to teach is inspirational.

I am indebted to Peter van Keken for providing me with advice and support from the day I stepped into Introduction to Geology to the review of this thesis. Ben van der Pluijm co-advised this project and taught one of my favorite classes, Earth Structure, which deepened my enthusiasm for geology and drove me to learn more. Graduate students Erin Lynch and Austin Boles have been fantastic instructors and have provided endless guidance throughout my time in the department. Lastly, I am so grateful for the unwavering love and support from my friends and family.

Thank you and forever Go Blue.

Abstract

There is an increasing number of paleomagnetic studies on the presence of chemical remanent magnetizations (CRMs) of sedimentary rocks, which can be interpreted as forms of remagnetizations. The link between deformation events and age of remagnetization is intriguing, but a mechanism to describe the correlation is still in discussion. The paleomagnetic fold test aims to determine the presence and timing of remagnetizations, relative to the deformation event. Specifically, syn-folding remagnetizations are studied to link timing of fold events, further constraining a possible age. In this study, a paleomagnetic analysis of the Sierra Madre Oriental, which includes regional fold tests and great circle analyses, was designed to present evidence for regional syn-folding. Due to weakly magnetized carbonates and the possibility of lightning induced IRM, the outcome includes varying data and few meaningful interpretations. However, field-induced IRM curves combined with stepwise thermal demagnetization indicate the presence of goethite, magnetite and possible laboratory-induced growth of a mineral in the samples. Also, many of the samples indicate a present day field component with a large north and downward vector, which is likely acquired through a viscous process and is apparent in the Zijderveld plots. A laboratory study revealed an increase in magnetic intensity when the samples were outside of magnetically shielded room, thus indicative of the possibility of viscous remanent magnetization (VRM) as an explanation of the sizable present day field component.

Introduction

Secondary magnetizations, which include remagnetizations, occur in magnetic minerals in the presence of a magnetic field when the minerals undergo chemical changes, or when they are subject to elevated temperatures. Remagnetizations in carbonate rocks did not become a fully recognized phenomenon until the 1980s (Van der Voo & Torsvik, 2012). Earlier studies explained mechanisms as thermoviscous remagnetizations (Kent, 1985) or mechanical rotations of magnetizations (van der Pluijm, 1987; Kodama, 1988). More recent studies present the mechanism for remagnetizations as chemical remanences that grow in stable single-domain magnetite grains, possibly during folding events (Weil & Van der Voo, 2002; Elmore *et. al*, 2001).

The few studies completed in Sierra Madre Oriental in northern Mexico indicate regional rotations, and possibly the presence of remagnetizations. Several previous paleomagnetic studies inferred that the magnetic remanence in the area is detrital. However, more recent studies indicate that this is improbable. Kleist *et. al* (1984) reasoned that three well-defined reversed-polarity intervals should be represented in the Sierra Madre Oriental, but observed only normal polarity (along with some anomalies). This suggests a younger (secondary) magnetization as the explanation for the failure to match the global geomagnetic polarity time scale. In addition, Nowicki *et. al* (1993) reported a syn-folding remanence magnetization of Eocene age in the Sierra Madre Oriental and Clement *et. al* (2000) also indicates remagnetized sections.

The purpose of this study is two-fold: to confirm a viscous remanent magnetization (VRM) acquisition (and decay) in the Sierra Madre Oriental samples, and to analyze and characterize the remanent magnetizations of the samples, ultimately in search of regional syn-folding. Syn-folding remanence directions, possibly due to smectite to illite transformations

resulting in magnetite growth and CRMs, coupled with age dating techniques can further constrain ages of remagnetizations, thus time intervals of regional geologic events.

Methods

Sampling

In 2014, Dr. Elisa Fitz-Diaz and Dr. Gabriel Chávez collected 33 sites (1-33) in the Monterrey Salient portion of the Sierra Madre Oriental, portrayed by **Figure 1c**. Here, the Sierra Madre Oriental is a 100-250 km wide fold belt located in the Mexican Fold-Thrust Belt (MFTB), which stretches dominantly N-S throughout Mexico (Campa-Uranga, 1983; Eguiluz et al., 2000). At the Salient, the trend of the belt changes northward from N-S to E-W (as seen in **Figure 1c**). The cores in this study are limestone from the Cupido and Tamaulipas formations, and are Barremian-Aptian in age. The region of study is dominated by flexural folds (km-scale), which have little local variation in the fold geometry.

A portable Pomeroy EZ Core Drill was used to collect six to ten core samples per site. The sample azimuth and plunge was measured using a Brunton compass and inclinometer. The site bedding, strike and dip, was measured also using a Brunton compass. In this study, 11 of the sites were used for analysis: 1, 2, 3, 4, 7, 8, 18, 30, 31, 32 and 33 (**Figure 1**).

The declination deviation value of 6°E was added to field azimuths of the samples. This value is based on the National Geophysical Data Center (NGDC) calculator from the United States National Oceanic and Atmospheric Administration (NOAA). It was measured on June 26th, 2013 using the latitude 25°33'13.043"N and longitude 100°38'44.8"W , which is a central location of the sampling area.

Laboratory

The cores were shipped to the Paleomagnetism, Structure and Tectonics Laboratory (PaSTeL) at the University of Michigan and were cut into 2.5 cm length specimens with a dual bladed saw. Thus, a core becomes a sample with up to 3 specimens. The azimuths of the specimens were marked with arrows in the downward plunge direction in the field, and again in the laboratory with Velvet Underglaze non-magnetic temperature resistant paint. Any specimens that were broken were glued together using alumina cement.

The natural remanent magnetizations (NRMs) were measured using a 2-G cryogenic magnetometer, followed by AF (alternating field) or thermal demagnetizations of the specimens in a magnetically shielded room in PaSTeL, to minimize an unwanted viscous magnetization acquisition. The specimens were thermally demagnetized with incremental steps using an ASC TD-48 demagnetizer located in the shielded room with a residual field of < 200nT. The specimens were stepwise heated to approximately 510°C, or until a spike in the magnetization was observed due to mineral alteration upon heating. Results of the demagnetization process were analyzed with orthogonal vector diagrams (Zijderveld, 1967), in stereographic projections, and magnetic moment diagrams using Paleomac software developed by Cogné (2003). Principal Component Analysis (PCA) was used with the Zijderveld plots for statistical analyses of the magnetic directions, along with Fisherian statistics. In addition, the Maximum Angular Deviation was calculated for each sample, which is represented by a best-fit line through the demagnetization vector (Kirschvink, 1980).

Viscous Remanent Magnetization - Experimental Methods

From the sample collection from the Sierra Madre, 15 specimens were randomly selected to test for an acquisition of a VRM. Inside a shielded room, there is only a minimal geomagnetic

field and little or no acquisition of a VRM, only decay of a previous VRM. Outside the shielded room, the geomagnetic field is present and allows for growth of a VRM. The samples were placed inside the shielded room for 16 weeks followed by 16 weeks outside of the shielded room, in turn followed by 3 weeks back inside the shielded room. The magnetic intensity of the samples was measured and recorded incrementally outside of the shielded room and weeks after being placed inside the shielded room.

Viscous Remanent Magnetization (VRM) Theory

Viscous remanent magnetization (VRM) is acquired when ferromagnetic minerals of a certain grain size are exposed to a geomagnetic field for a duration of seconds to years to millions of years. Natural VRMs are in the form of secondary remagnetizations that are slowly acquired records of the present day field. In single domain-type samples (SD), the magnetic moments of the grains with a short relaxation time are realigned repeatedly in order to seek equilibrium, and a VRM is acquired in the direction of the applied magnetic field. The acquisition of the remanence is a function of time and increasing volume. With pseudo-single domain (PSD) and multidomain (MD) grains, a VRM is acquired by thermal energy that activates and displaces domain walls. In MD grains, there is generally an inverse relationship between grain coercivity and viscosity (i.e. with a lower coercive force, VRM is acquired more rapidly and vice versa). The VRM in samples is often considered irrelevant and is discarded through identification in low-field demagnetization steps (Butler & Butler, 1992).

VRM depends on magnetic relaxation, which occurs due to thermal energy that decays the magnetic remanence in SD grains. Temperature plays a large role in relaxation time. Both the coercive force (h_c) and the (saturation) magnetization (j_s) depend on temperature (j_s goes to zero at the Curie temperature of the grains). Louis Neél described the magnetic relaxation time as:

$$\tau = 1/C \exp (vh_c j_s/2kT)$$

C= Frequency factor $\sim 10^8$ s^{-1}

v= volume of SD grain

h_c= microscopic coercive force of SD grain

j_s= saturation magnetization of the ferromagnetic material

kT= thermal energy (k is Boltzmann's constant)

Neél Equation
We recognize, from this Neél equation, that the relaxation time gets to be longer with (1) larger volume, (2) greater coercivity, (3) higher saturation moments, and (4) lower temperature. A greater τ implies a higher/longer stability and retention of remanence.

The magnetic relaxation time can also be expressed as the ratio of blocking energy ($vh_c j_s$), which is the amount of energy required to rotate j_s, to thermal energy (kT). Grains with a low vh_c have a low relaxation time and the opposite is true for grains with a high relaxation time (Butler & Butler, 1992).

VRM is acquired through realigning magnetic moments of grains with a relatively short relaxation time, τ. SD grains are "unblocked" if the relaxation time, τ, is less than (or equal to) the acquisition time of the VRM, and can realign to the present or applied magnetic field and reach an equilibrium. When τ = acquisition/relaxation time increases, VRM increases/decreases as well. **Figure 2** portrays this phenomenon on a diagram of grain volume, v, versus coercive force, h_c. Again, as τ=acquisition time increases (bold line) through the SD grain distribution, VRM follows with an increase (Butler & Butler, 1992).

For MD and PSD grains, VRM is acquired in the direction of the applied magnetic field due to thermal activation and displacement of the domain walls. The coercive force, h_c, decreases (increases) with increasing (decreasing) temperature and enough energy is applied to allow realignment of magnetic moments, or VRM. In MD grains, a low coercive force allows for VRM acquisition as well.

8

Experimental data portrayed in **Figure 3** represents a VRM acquisition at different

temperatures. A sample with magnetite grains that are 2-µm in size was placed in a 3.3 Oe (0.33

mT) magnetic field. VRM acquisition was measured continually over time

$$\text{VRM} = S \log t$$

where S is the viscosity coefficient and t is the duration over which VRM is acquired, or the

acquisition time (seconds). The increase in VRM over time indicates that the most recent

magnetic field in which the sample was placed induces a viscous magnetization (Butler & Butler,

1992).

Natural remanent magnetization (NRM) is the remanent magnetization in a rock that can

be measured by magnetometers before laboratory treatment. More than one component usually

makes up the NRM: the "primary NRM", which is the remanent magnetization acquired when

the rock was formed, and the "secondary NRM", which can be acquired significantly later than

rock formation (Butler & Butler, 1992). VRMs and NRMs can have comparable magnitudes;

consequently, VRMs can contaminate or mask the record of the ancient geomagnetic field or the

"primary NRM" that is usually of interest (Yu & Tauxe, 2006).

Exposing rocks to cooling temperatures below the Curie temperature for a long duration

of time can form a thermoremanent magnetization (TRM) or a thermoviscous remanent

magnetization (TVRM), which can be primary as well as secondary remanence. Acquisition of

TVRM in SD grains depends on a relaxation time-temperature relationship. The coercive force

as a function of temperature $h_c\ (T)$ is necessary to understand this relationship.

$$h_c\ (T) = \Delta N_D j_s\ (T)$$

$\Delta N_D =$ difference in internal demagnetizing factor between short and long axes of the SD particle

9

Blocking diagrams show the relaxation time-blocking temperature relationship, (τ, T_B), for SD grains through laboratory times and temperatures, correlating with geologic times (Butler & Butler, 1992). However, these blocking diagrams are inapplicable for PSD magnetite grains (Borradaile, 1999). Point 1 on **Figure 4** shows the conditions when SD magnetite grains may acquire a VRM in nature, i.e., when the grains are exposed to a geomagnetic field at 260°C for 10 million years. These conditions are typical for natural (burial) conditions of the rocks. Point 2 shows, in contrast, the relationship of these same SD magnetite grains acquiring a VRM if exposed for 30 minutes at 400°C in the laboratory. These points are on the same τ-T_B nomogram line, which indicates that the remanence of these grains be acquired either at τ=10 million years at 260°C or τ=30 minutes at 400°C or points in between. Conversely, the NRM of the grains can be unblocked by a temperature of 400°C for 30 minutes in zero magnetic field, erasing the magnetization. The nomogram lines on the blocking diagram show that at higher temperatures, it requires a smaller amount of temperature increase to unblock the grains. Closer to the Curie temperature, there is a rapid decrease (points 4 to 3) in relaxation time with an increase in temperature ("A" region). The "B" region of the blocking diagram represents grains that likely acquire secondary TVRM or VRM and not primary components of magnetization because they have blocking temperatures at least 100°C below the Curie temperature. However, the "A" region has blocking temperatures within 100°C of the Curie temperature and often obtain a primary TRM since rocks require heating close to the Curie temperature to alter the magnetization (Butler & Butler, 1992).

Thermal demagnetization is a technique used to first erase secondary NRM, such as a TVRM, and then the primary NRM at higher temperatures. Heating up specimens to a temperature T_B (below the Curie temperature) and then cooling them in a zero magnetic room

allows the specimens to lose the TRM below T_B (**Figure 5**). TVRM shows that SD grains of

secondary NRM have a short τ and a low blocking temperature (T_B) and this component can be

removed by heating below the blocking temperature of the grains of the primary NRM. **Figure 5**

shows a v-h_c diagram in which grains with a low T_B (and a short τ) tend to acquire VRM rather

than a primary or so-called characteristic remanent magnetizations (ChRM). Thermal

demagnetization as a technique for erasing VRM (without affecting ChRM grains with longer τ

and high T_B) requires temperatures that are less than and/or equal to the blocking temperatures of

the VRM-carrying grains. This technique applies to SD grains; the presence of PSD grains can

alter the TVRM relationship and has at this time yet to be expressed as a comparable theory

(Butler & Butler, 1992).

Viscous Remanent Magnetization – Experimental Results

     Many of the samples portray a clear decrease in the magnetic intensity at the last point,

which is preceded by 3 weeks inside the shielded room, thus allowing a decrease in magnetic

intensity. Seen in **Figure 6**, most of the specimens portray a very slight increase in magnetic

intensity over the weeks outside the shielded room, followed by a clear decrease in magnetic

intensity once placed back inside the room (e.g., portrayed by SM9-6a). Some of the samples

show a steady magnetic intensity throughout the experiment (portrayed by SM14-7), indicating

grains without size distribution amenable for VRM acquisition.

Fold Test Theory

Field tests of paleomagnetic stability provide information on the timing of acquisition of

the ChRM (characteristic remanent magnetization), whereas laboratory tests cannot provide such

information. The fold test is an example of a paleomagnetic stability test that provides

information on the relative timing of acquisition of a ChRM component. If the in-situ directions

11

(geographic coordinates) or their paleomagnetic poles are significantly dispersed but become clustered upon application of the bedding correction, then the ChRM is most likely acquired before a folding event (pre-folding). This is considered to be a "positive fold test", represented by **Figure 7a,** and the remanence is mostly likely considered primary (Watson & Enkin, 1993). If the fold test portrays in-situ directions (geographic coordinates) that are clustered and become more scattered upon unfolding, then we assume the ChRM was acquired post-folding, and this is considered to be a "negative fold test", indicating that the rocks were (re)magnetized, and that the remanence is secondary (Watson & Enkin, 1993) (Butler & Butler, 1992).

The validity of fold tests relies on statistical significance. The significance of the dispersion of magnetic directions is portrayed by a few parameters. The k value, or Fisher precision parameter, represents either the tightness of clustering or its inverse, the dispersion of the directions. The k value is defined as $k=(N-1)/(N-R)$ where N is the number of entries and R is the resultant vector sum of the entries (McFadden & Jones, 1981). A higher k value indicates tighter clustering (McElhinny, 1964). The ratio of the k values is derived from data obtained before, k_1, and after, k_2, structural correction (Watson & Enkin, 1993). A larger k_2/k_1 is considered a "positive fold test", when directions are more clustered after a structural correction. The precision parameter, k, is often portrayed as a function of the percent of untilting; this version is called an "incremental fold test". For syn-folding magnetizations, or magnetizations that are acquired before the completion of the folding event, k is highest at some point between zero and 100% untilting. McElhinny (1964) specified that for a hypothesis with a 95% significance level, the hypothesis be omitted if data within 5% present the null hypothesis to be true. Therefore, k values that have significance levels greater than 95% are used.

Recent studies increasingly have shown syn-folding magnetizations, illustrated in **Figure 7b** (Butler & Butler, 1992). Pre-folding and post-folding acquisitions of magnetizations in an isoclinal fold portray parallel magnetic directions, or the tightest clustering of paleomagnetic data, in the two observed limbs, whereas syn-folding magnetizations portray parallel magnetic directions at an intermediate stage of unfolding. The magnetic grains are blocked during folding, and any preexisting magnetizations are replaced. However, "apparent syn-folding" is possible if there are preexisting magnetizations that are not replaced, i.e., when the timing of the remagnetizations does not coincide with the maximum clustering. Apparent syn-folding can also be portrayed if the structural history of the area is not completely understood, and inaccurate structural corrections are applied (Lewchuk et. al, 2003).

Syn-folding remagnetizations can be a result of a variety of mechanisms. Chemical remanent magnetizations (CRMs) are frequent in sedimentary rocks and are often characterized by syn-folding remagnetizations. CRMs are acquired in the presence of a magnetic field from chemical reactions that produce ferromagnetic minerals, often magnetite, below their blocking temperature (Butler & Butler, 1992). Alternatively, CRMs may be acquired when nano-scale Fe-oxide grains grow in size above the SP-SD threshold. Important for this study, a mechanism for CRMs, which still requires more testing, is through the migration of orogenic fluids as a result of folding, which initiate the chemical reactions, following the release of iron, which in turn will precipitate as ferromagnetic grains and the build up of a remagnetization (Elmore et al, 2001). The timing of the syn-folding remagnetization suggests a link with the age of the folding event (Gill et. al, 2002)

The incremental fold test examines greater or less clustering of ChRM directions incrementally through the application of untilting (also known as "the bedding correction"). The

method of untilting to find the maximum *k* value includes plotting the means of the directions and their statistical parameters from two or more sites, for example from opposing limbs of a fold, while applying a partial structural correction that depends on the bedding. The largest *k* value occurs where the mean directions of the two or more sites merge upon structural correction, and become statistically most clustered together. Instead of a comparison of site mean directions, the test can also be carried out with sample directions. An example of the merging of directions is shown in **Figure 7c** and the maximum clustering of the samples (or sites) is shown in **Figure 7d** (Butler & Butler, 1992). The percentage of untilting that coincides with the largest *k* value should be statistically significantly different from zero or 100% untilted distributions. **Figure 7b** shows the magnetizations are aligned when they are partially folded and **Figure 7d** shows the maximum clustering, or the direction where the magnetizations of **Figure 7b** are aligned (Butler & Butler, 1992).

Directional Analysis

Incoherent Directions

The sites sampled for the study provide varying data and many inconclusive results. Unfortunately, few site-means have been useful candidates for interpretation. The samples in this study were all thermally demagnetized, but cut specimens from large cores have also been demagnetized with the alternating field (AF) method. Upon comparison of the AF and thermal method of demagnetization, it is apparent that the AF method conceals, partially or completely, components of magnetization that thermal demagnetization clearly exhibits. See **Figure 8**, where two specimens from the same core are compared using the two methods of demagnetization. The AF specimen portrays a nearly univectorial magnetic decay, or deceptively one component of magnetization, whereas the thermally demagnetized specimen shows two components (one of

14

which is the present day field). It is likely that the Zijderveld plot of the AF-treated sample portrays a combination of both. The simultaneous removal of the two components becomes apparent only in the thermally-treated specimen. Therefore, thermal demagnetization was solely used in the remainder of the sample treatments, in order to isolate the ChRM in the most accurate way.

The carbonates in this study were weakly magnetized, which often manifested in messy zigzag stereographic projections and unsystematic Zijderveld plots of samples. **Figure 9**, which represents this type of chaotic Zijderveld plot and lack of clustered points in the stereographic projection, fails to approximate the decay of any magnetization. In contrast, many other samples portray clean, univectorial decay of magnetizations (**Figure 10**). These Zijderveld plots with low MAD angles and clustered magnetic directions on the stereographic projection prompt us to do further analysis and interpretation.

Present-day Field Directions

An overprint that represents a present day field (PDF) component, likely a VRM, is apparent in many samples in this study and is represented by a large northerly and downward component first removed on the Zijderveld diagram (see Table 1). **Figure 11** (left) provides an example of the presence of the VRM component, which is removed first leaving only the ChRM (**Figure 11**-right) in the sample, which is used for analysis. The thermal demagnetization temperatures that most commonly indicate the PDF include 20° to 200°C. The vector that represents these lower temperatures is removed (**Figure 11**-right). Importantly, the presence and direction of this PDF component confirms that samples were properly oriented and that this component is unlikely influenced by lightning strikes.

15

When the samples in the study yield varying magnetic directions within a site, the site means in this study have obviously low precision of magnetic directions. For example, **Figure 12** portrays a site mean where no preference can be held for the sample directions within the site, even though they might present occasional clustered sample directions. It is possible that lightning struck this area, as it would have magnetized the site in no particular pattern, and would present samples that have clean, univectorial decay of magnetizations, high k value, and no PDF component. Site 32 (**Figure 12**) contains a mix of samples that contain a PDF overprint (not portrayed in the figure) in addition to samples that do not contain this overprint (portrayed in **Figure 12**), which instead portray a clean univectorial decay of magnetization with a direction other than PDF and a high k value (for the sample). Even though some samples within this site exhibit highly clustered directions, overall the magnetic directions within this site are too incoherent and a statistically significant site mean cannot be determined. Sites that are highly imprecise, such as this one, cannot be used for further analysis with respect to this study. The directions of these samples do not align with each other and do not have a clustered site mean. Moreover, they often do not contain a PDF and the samples individually have a high $k,$ all of which indicate the possibility of lightning induced IRM.

Coherent Directions

Many of the sites in this study have site means that are based on well-clustered directions, and the samples contain systematic PDF overprints (see **Table 1** for a complete list). For instance, site 30 reveals highly clustered magnetic directions of the samples, which contain a consistent PDF overprint (**Table 1**, **Figure 13**) that is removed from the plot in **Figure 13** (far right) in order to show the remaining ChRM component, which is then used to derive site means.

Such a site represents consistency of the samples within the site and allows for further analysis for this study.

Great Circle Analysis

Demagnetizing a sample with two components of magnetization can result in directions that span a great circle path rather than a cluster of points that represent a single (univectorial) direction (McFadden & McElhinny, 1988). The two actual directions lie in the plane of the great circle, and fall somewhere along the great circle path. An intersection with more than one great circle is necessary to obtain information on one of the two unknown directions. Moreover, great circle analyses that can be combined with directional observations usually provide reliable directions. In addition, intersections of great circles at larger angles (more orthogonal to each other) are needed to provide more reliable information. The precision parameters k for great circle and direct observation analyses are given as (McFadden & McElhinny, 1988):

$$k=[2M + N - 2]/[2(M + N - R)]$$

M: number of direct observations

N: number of great circles

R: resultant vector of [N+M]

Certain sites in this study represent the need for great circle analysis, as the measured directions show a streaking pattern and are too scattered for the application of Fisherian statistics exclusively (but great circles can use Fisherian statistics once the circle is determined). **Figure 14** represents a site that has sample directions along a great circle path. Thus, the true ChRM mean direction of the sites falls somewhere on the plane represented. The normal (or the pole to the great circle plane) is used for paleomagnetic analysis.

Fold Test Analysis

The fold test can provide relative timing of the acquisition of the magnetization of two or more sites in question, which are located in areas with different bedding. It is important to note that if a fold test is applied to samples of the same bed on two limbs, the bed's two sites should have the same polarity upon appropriate bedding correction. In addition, in the coordinates of the bedding correction that produces maximum k, the site mean directions should be the typical directions of the geomagnetic field in Mexico, which are generally northerly and downward directions or southerly and upward directions.

Figure 15 and **16** represent two sites of normal polarity in the general northwest and downward direction; site 33 is represented with a great circle. Upon structural correction, the sites become less clustered and site 33 changes polarity, indicating that magnetizations were acquired after the fold event, also known as a negative fold test.

Figure 17 represents two sites that are located on opposing limbs, and provide a fold test, as shown in **Figure 18**. Site 3, which is the site that is northwest and upward, is well clustered and site 2 is represented with great circles and sample means that trend northward. A fold test with both sites is statistically insignificant, as is common for the application of the fold test on multiple sites in this study. In order to achieve a more significant fold test, one sample direction from site 2 was chosen for a fold test with site 3 (chosen sample is represented with a star on the stereographs). The site 2 sample direction used in the fold test was chosen based on its northerly direction, and it converges most with the site 3 sample directions upon structural correction. The resultant fold test has a higher k value since the two sites (site 2 with only one sample direction) are somewhat clustered.

Figure 19 and **20** portray a fold test with two sites on opposing limbs and opposite polarities. However, this fold test portrays pre-folding acquisition of magnetizations. The site means become most clustered in the general southeast and upward direction close to 100% of the structural correction, which suggests that the magnetization was acquired before or at the beginning of the folding event. This indicates the possibility of the remanence as primary. The precision parameter, k, is relatively high as most of the samples were eliminated, leaving only 3 sample directions used from site 7, which provides more clustering after tilt correction. **Figure 21** portrays two sites on opposing limbs and opposing polarities and the corresponding fold test (**Figure 22)** shows a syn-folding magnetization. There is a possibility that one of the two sites became magnetized in a time of reversed polarity. So, **Figure 23** portrays one site, site 18, with inverted polarity and the site on the opposing limb, site 30, remaining unchanged, making the polarity the same, with intent of yielding a statistically significant fold test (**Figure 24**). The maximum clustering, or k, in the syn-folding fold test occurs in the general south/southeast and upward direction. Unfortunately, both fold tests (**Figure 22** and **Figure 24**) are very similar and yield statistically insignificant results.

The fold test results lack the ability to link remagnetizations with fold events. Interestingly, there is a geographic distribution. The post-folding remanence is located on the western portion of the Monterrey Salient, the syn-folding remanence occurs in the mid-section, and the two pre-folding remanences occur in the N-S portion of the belt, or the most eastern portion the sampled area.

Magnetic Mineral Characterization ("Lowrie Test")

In order to determine the ferromagnetic minerals in a sample by Curie temperature, a three-component isothermal remanent magnetization (IRM) curve combined with stepwise

thermal demagnetization is analyzed, so that differing coercivities and magnetic unblocking can be revealed and correlated. A strong magnetic field is necessary for magnetic analysis in order to reach saturation magnetization of the minerals. Minerals can have similar coercivities, but differing unblocking temperatures, demonstrated through thermal demagnetization steps (Lowrie, 1990).

The thermal decay of the IRM indicates the minerals present. The decay of the magnetization of the minerals varies depending on the types of minerals and their unblocking temperatures. In this study, magnetizing fields at 120mT, 300mT and 1000mT were induced in three orthogonal directions respectively. A field of at least 1000mT is necessary to magnetize all common ferromagnetic minerals (Lowrie, 1990). Thus, 1000mT was induced in one direction, followed by 300mT in an orthogonal direction. The 300mT field remagnetized the coercivity fractions softer than 300mT, the maximum for magnetite, leaving the higher coercivity fractions magnetized along the directional axis of the 1000mT field. Lastly, the 120mT induced field remagnetized the components softer than 120mT, leaving the higher coercivities magnetized as before. Then, the samples were thermally demagnetized in a near-zero-field room.

The IRM curves **(Figures 25** and **26)** portray three different symbols, namely squares, triangles and circles, which represent the three orthogonal vectors and the coercivities of minerals with the applied magnetizing fields at 1000mT, 300mT and 120mT respectively. The IRM curve of **Figure 25** shows a sharp drop at 100 degrees Celsius of the square component (the hardest component), and a small drop of the triangle component (medium component). A high coercivity and low unblocking temperature (around 150 degrees Celsius) such as this indicates the presence of goethite. After the sharp drop, the other fractions demagnetize smoothly until 510 degrees Celsius, indicating the presence of magnetite. On the other hand, the IRM curve of

20

Figure 26 shows a slight decay of the square component and larger decay of the circle and triangle components. There is generally a smooth decay of magnetization until 640 degrees, indicating the presence of hematite, which could possibly be a high temperature laboratory induced oxidation product.

Conclusion

The ambiguous evidence for syn-folding magnetizations, abundance of varying data and inconclusive results, led to few meaningful interpretations and plenty of frustrating stretches in time. But, important aspects were revealed regarding laboratory methods and paleomagnetism in the Sierra Madre Oriental. Weakly magnetized carbonate samples provide hardships for acquiring statistically significant sample directions and site means. Subsequently, applying paleomagnetic field tests to these incoherent samples, such as fold tests and great circle analyses, often results in statistically insignificant or ambiguous outcomes. The results do not provide evidence for rotations. However, from the fold tests, there are four (somewhat) meaningful results that portray a post-folding remanence with normal polarity, two pre-folding remanences with reversed polarities, and a syn-folding remanence with a reversed polarity. These indicate the possibility of primary or remagnetized remanences, but the results remain inconclusive because of the dispersed character of site means and low k for the fold tests. The remanence location distribution could be studied further for correlations with tectonic events.

The behaviors of the samples possibly represent MD or borderline SD grains since the magnetic field was acquired relatively quickly, indicating presence of a lower coercive force and MD grains. Thus, this could link to the present day field component seen in most of the samples, confirming it as a viscous acquisition. Chaotic site means that include samples with clean decay of magnetizations, univectorial directions and no present day field components can indicate

21

lightning induced IRMs, since there are no preferential directions. Laboratory induced hematite

formation may be due to oxidation of Fe_3O_4 to Fe_2O_3, which could justify the high temperature

needed to completely decay magnetizations in one sample studied. Lastly, it is important to note

for future studies that the AF method of demagnetization conceals partially or completely

components of magnetization that are apparent in thermal demagnetizations.

References

Borradaile, G. J. (1999). Viscous remanent magnetization of high thermal stability in limestone. *Geological Society, London, Special Publications*, *151*(1), 27-42.

Butler, R. F., & Butler, R. F. (1992). *Paleomagnetism: magnetic domains to geologic terranes* (Vol. 319). Boston: Blackwell Scientific Publications.

Campa-Uranga, M. F. 1983. The tectonostratigraphic terranes and the thrust belt in Mexican territory; Proceedings of the Circum-Pacific terrane conference. Stanford University Publications. Geological Sciences, 18, 44-46.

Clement, B. M., Poetisi, E., Bralower, T. J., CoBabe, E., & Longoria, J. (2000). Magnetostratigraphy of mid-Cretaceous limestones from the Sierra Madre of northeastern Mexico. *Geophysical Journal International*, *143*(1), 219-229.

Cogné, J.P., 2003, PaleoMac: A MacintoshTM application for treating paleomagnetic data and making plate reconstructions. Geochemistry Geophysics Geosystems, 4:1-8.

Eguiluz, S.; Aranda-Gómez, M. and Marret, R. 2000. Tectónica de la Sierra Madre Oriental, México. Boletín de la Sociedad Geológica Mexicana, LIII, 1-26.

Elmore, R. D., Kelley, J., Evans, M., & Lewchuk, M. T. (2001). Remagnetization and orogenic fluids: testing the hypothesis in the central Appalachians.*Geophysical Journal International*, *144*(3), 568-576.

Gill, J. D., Elmore, R. D., & Engel, M. H. (2002). Chemical remagnetization and clay diagenesis: testing the hypothesis in the Cretaceous sedimentary rocks of northwestern Montana. *Physics and Chemistry of the Earth, Parts A/B/C*,*27*(25), 1131-1139.

Kent, D. V. (1985). Thermoviscous remagnetization in some Appalachian limestones. *Geophysical Research Letters*, *12*(12), 805-808.

Kirschvink, J.L., 1980. The least-square line and plane and the analysis of paleomagnetic data. Geophysical Journal of the Royal Astronomical Society, 62:699– 718.

Kleist, R., Hall, S. A., & Evans, I. (1984). A paleomagnetic study of the Lower Cretaceous Cupido Limestone, northeast Mexico: Evidence for local rotation within the Sierra Madre Oriental. *Geological Society of America Bulletin*, *95*(1), 55-60.

Kodama, K. P. (1988). Remanence rotation due to rock strain during folding and the stepwise application of the fold test. *Journal of Geophysical Research: Solid Earth (1978–2012)*, *93*(B4), 3357-3371.

Lewchuk, M. T., Evans, M., & Elmore, R. D. (2003). Synfolding remagnetization and deformation: results from Palaeozoic sedimentary rocks in West Virginia.*Geophysical Journal International*, *152*(2), 266-279.

Lowrie, W. (1990). Identification of ferromagnetic minerals in a rock by coercivity and unblocking temperature properties. *Geophysical Research Letters*, *17*(2), 159-162.

McElhinny, M. W. (1964). Statistical significance of the fold test in palaeomagnetism. *Geophysical Journal International*, *8*(3), 338-340.

McFadden, P. L., & McElhinny, M. W. (1988). The combined analysis of remagnetization circles and direct observations in palaeomagnetism. *Earth and Planetary Science Letters*, *87*(1), 161-172.

McFadden, P. L., & Jones, D. L. (1981). The fold test in palaeomagnetism. *Geophysical Journal International*, *67*(1), 53-58.

Nowicki, M. J., Hall, S. A., & Evans, I. (1993). Palaeomagnetic evidence for local and regional post-Eocene rotations in northern Mexico. *Geophysical Journal International*, *114*(1), 63-75.

van der Pluijm, B. A. (1987). Grain‑scale deformation and the fold test‑evaluation of syn‑folding remagnetization. *Geophysical Research Letters*, *14*(2), 155-157.

van der Voo, R., & Torsvik, T. H. (2012). The history of remagnetization of sedimentary rocks: deceptions, developments and discoveries. *Geological Society, London, Special Publications*, *371*(1), 23-53.

Watson, G. S., & Enkin, R. J. (1993). The fold test in paleomagnetism as a parameter estimation problem. *Geophysical Research Letters*, *20*(19), 2135-2137.

Yu, Y., & Tauxe, L. (2006). Acquisition of viscous remanent magnetization. *Physics of the Earth and Planetary Interiors*, *159*(1), 32-42.

Zijderveld, J.D.A., 1967. AC demagnetization of rocks: analysis of results. In: Collinson, D.W., Creer, K.M. (Eds.), Methods in Paleomagnetism. Elsevier, Amsterdam, 254– 286.
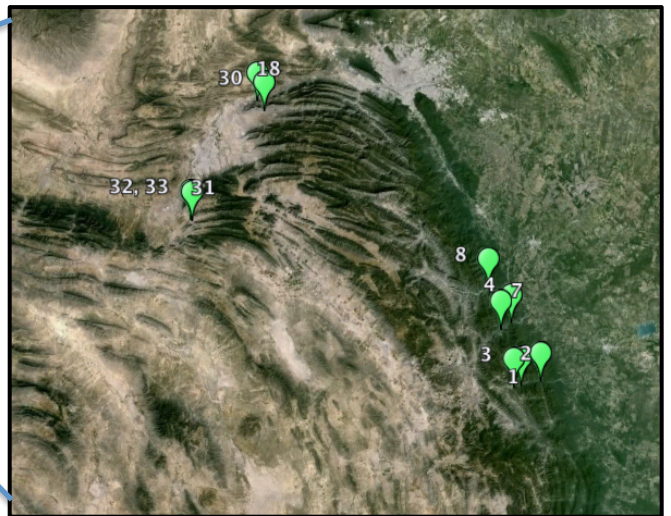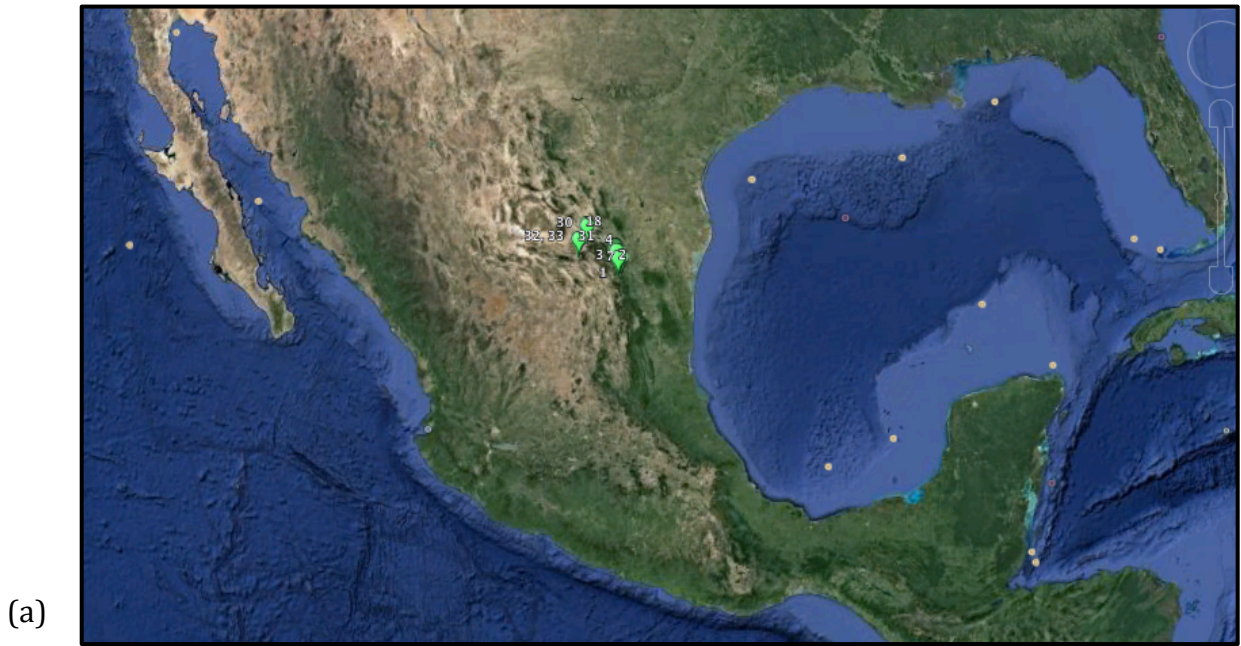
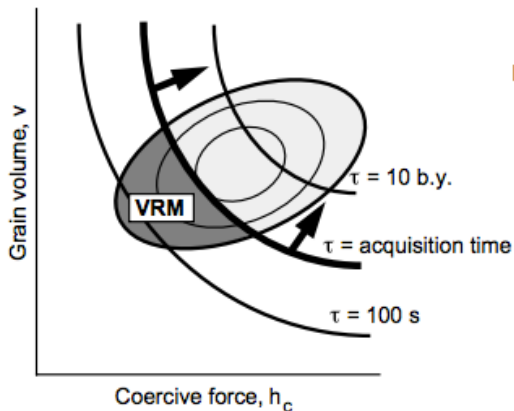**Figure 1:** Sampling area: (a) map of Mexico, (b) Sierra Madre Oriental and the (c)Monterrey Salient.

Figure 2: Schematic representation of VRM acquisition on a diagram of SD grain volume (v) versus microscopic coercive force (h_c). As the time of VRM acquisition increases, the bold line labeled "τ = acquisition time" sweeps through the SD grain population from lower left to upper right; grains with progressively longer τ can acquire VRM as acquisition time increases; SD grains in the dark region labeled "VRM" have acquired VRM. Figure from Butler & Butler, 1992.
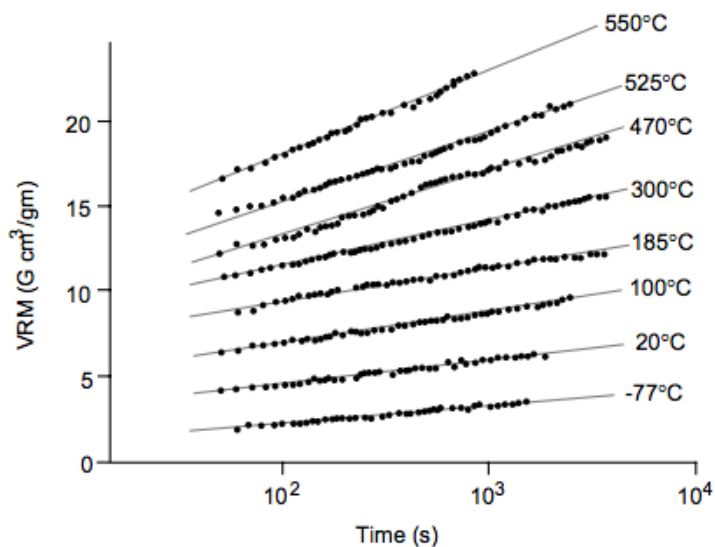
Figure 3: Progressive acquisition of VRM by synthetic sample of dispersed 2-mm diameter grains of magnetite. Data points show VRM acquired at corresponding time since the beginning of exposure to the magnetic field; lines show the trend of VRM for a particular VRM acquisition experiment at the temperature indicated; the magnetic field was 3.3 Oe; zero on the ordinate is arbitrary (the absolute value of VRM was adjusted so that results of all VRM acquisition experiments could be conveniently shown on a single drawing). Redrawn from Stacey and Banerjee (1974). Figure from Butler & Butler, 1992.
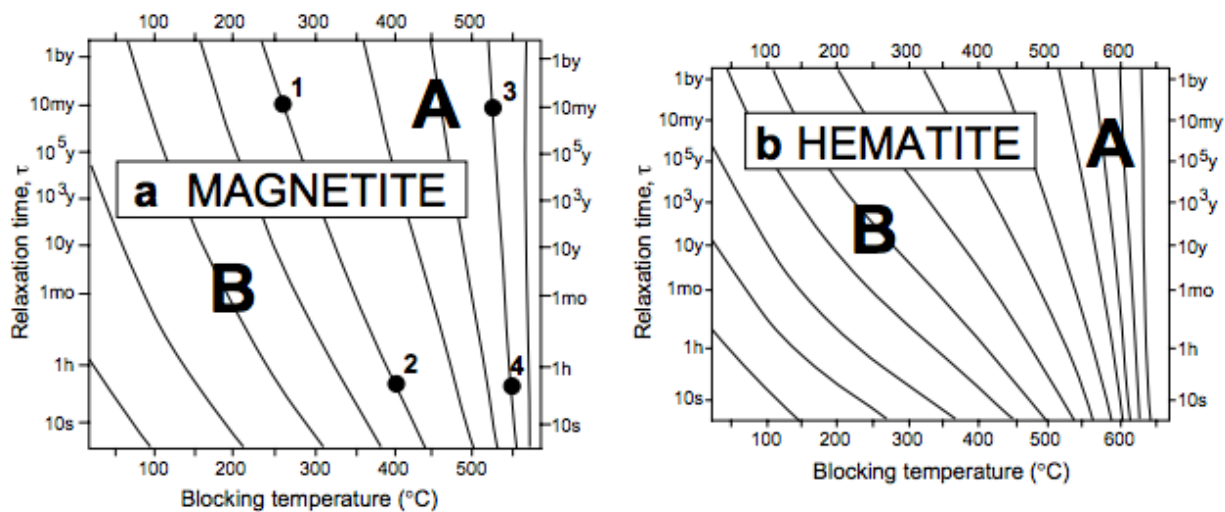

Figure 4: Blocking diagrams for (a) magnetite and (b) hematite. Lines on the diagrams connect combined temperature and relaxation time (τ) conditions that can unblock (reset) the magnetization in a given population of SD grains. See text for explanation. Redrawn from Pullaiah et al. (1975). Figure from Butler & Butler, 1992.
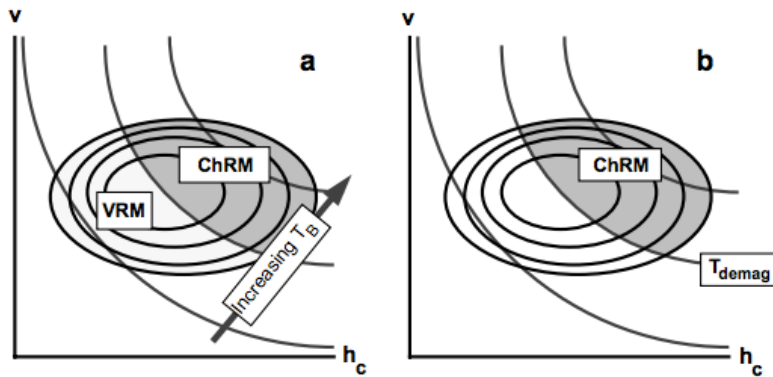
Figure 5: Schematic explanation of thermal demagnetization. (a) Diagram plots grain volume (v) versus microscopic coercive force (h_c) for a hypothetical population of SD grains. Solid contours are of concentration of SD grains; grains with low τ and low T_B preferentially carry VRM; these grains occupy the region in the lower left portion of the diagram; grains with high τ and high T_B preferentially carry ChRM; these grains occupy the shaded region. (b) Following thermal demagnetization to temperature T_{demag}, NRM in SD grains with $T_B < T_{demag}$ is erased. Only the ChRM in the SD grains with higher T_B remains. Figure from Butler & Butler, 1992.

Figure 6: These specimens were placed outside of the magnetically shielded room for 16 weeks, and then placed back inside the shielded room for 3 weeks. Magnetic intensity is plotted over the number of weeks to portray the viscous remanent magnetization acquisition and subsequent decay.
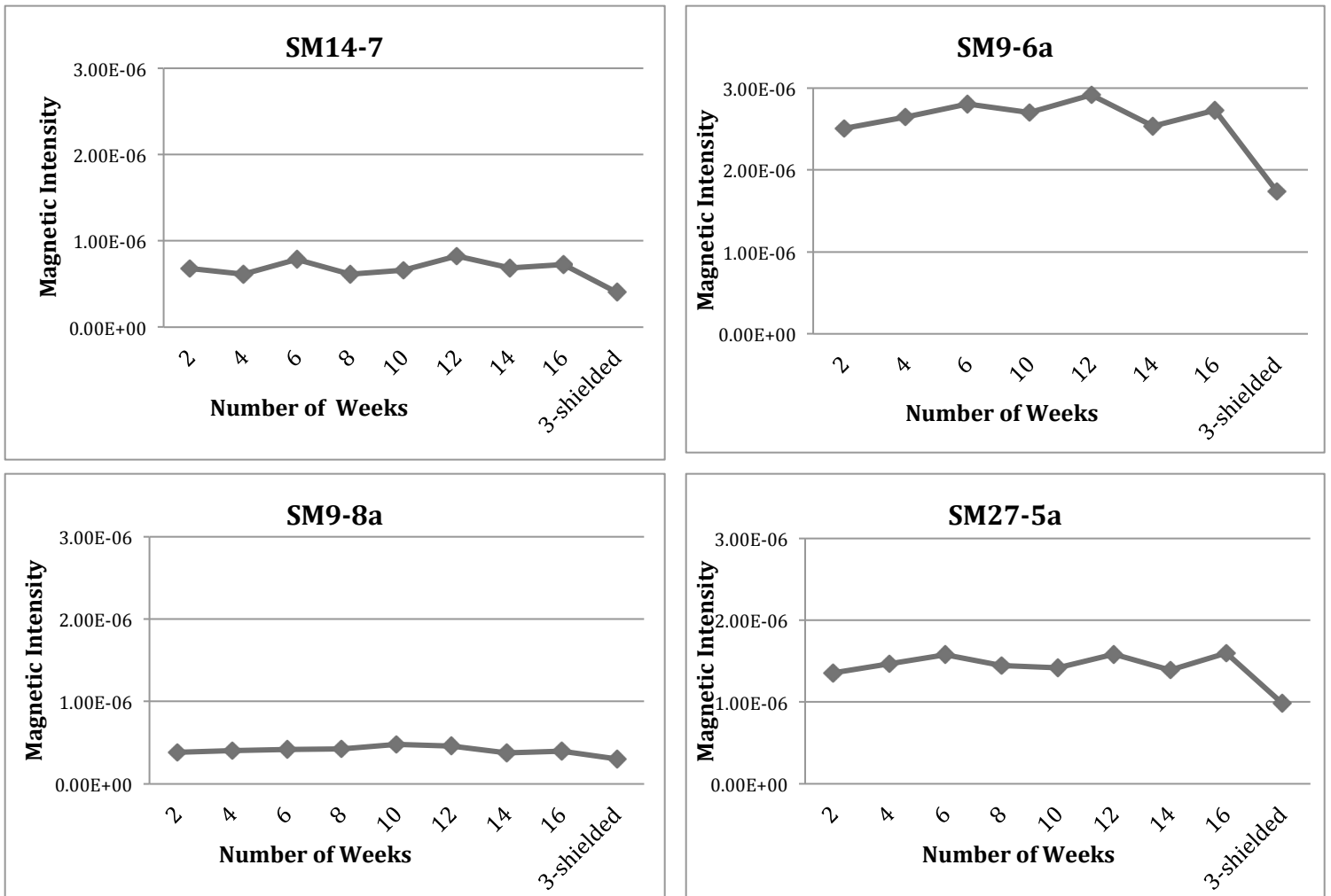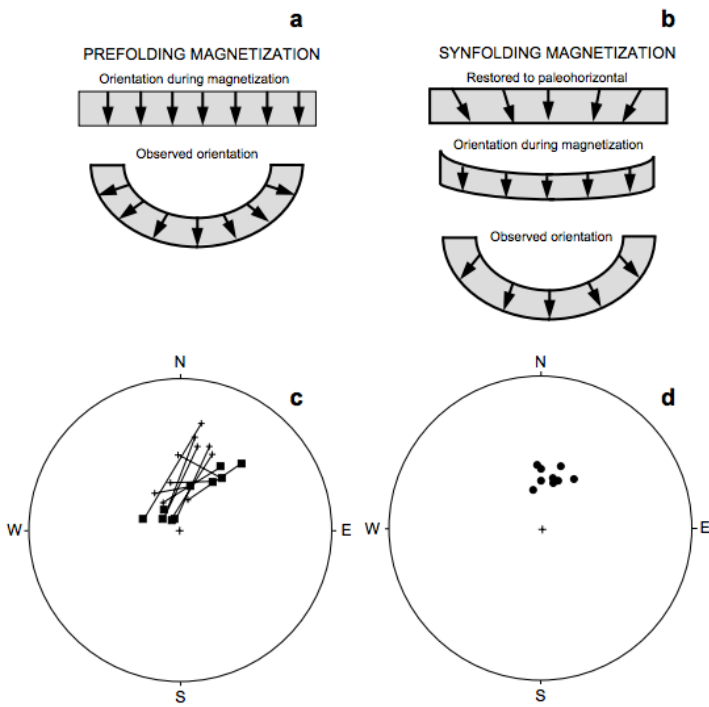
Figure 7: Syn-folding magnetization. (a) Directions of ChRM are shown by arrows for pre-folding magnetization. ChRM directions are dispersed in the observed in situ orientation; restoring bedding to horizontal results in maximum grouping of the ChRM directions. (b) Directions of ChRM for syn-folding magnetization. ChRM directions are dispersed in both the in situ orientation and when bedding is restored to horizontal; maximum grouping of the ChRM directions occurs when bedding is partially restored to horizontal. (c) Equal-area projection of directions of ChRM. Crosses are in situ site mean ChRM directions for ten sites spread across opposing limbs of a fold; squares are site mean ChRM directions resulting from restoring bedding at each site to horizontal; all directions are in the lower hemisphere of the projection. (d) Site-mean ChRM directions after 50% unfolding. Data from Bazard et al. (Can. J. Earth Sci., v. 27, 330–343, 1990). Figure from Butler & Butler, 1992.

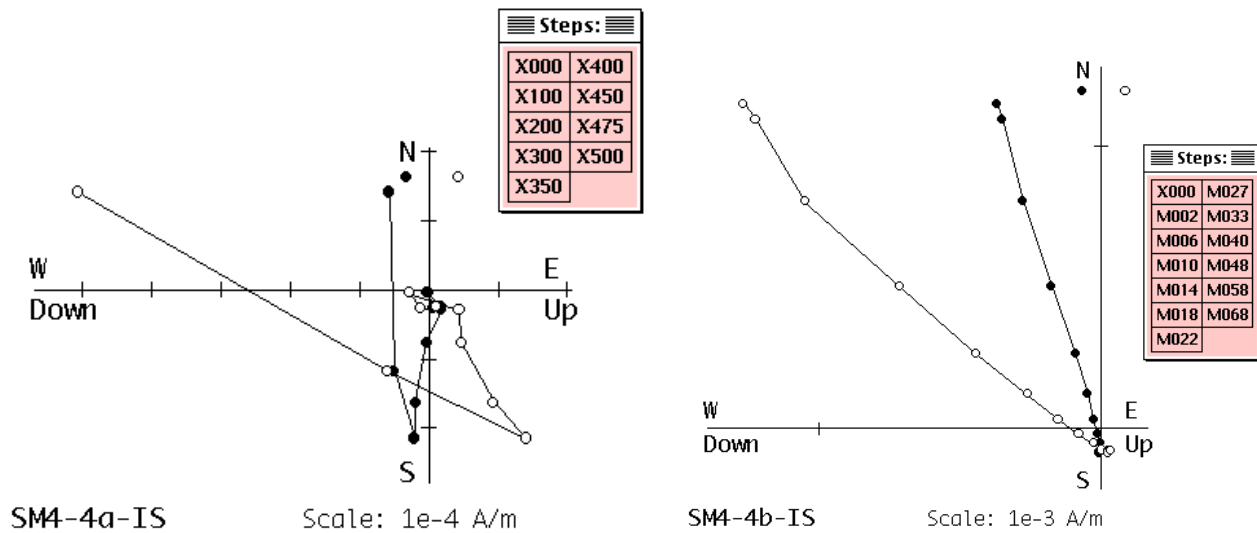
Figure 8: Comparison of thermal (left) and AF (right) demagnetization methods. The Zijderveld plot representing the thermal method reveals components of magnetization that the AF Zijderveld plot masks in a quasi univectorial decay.

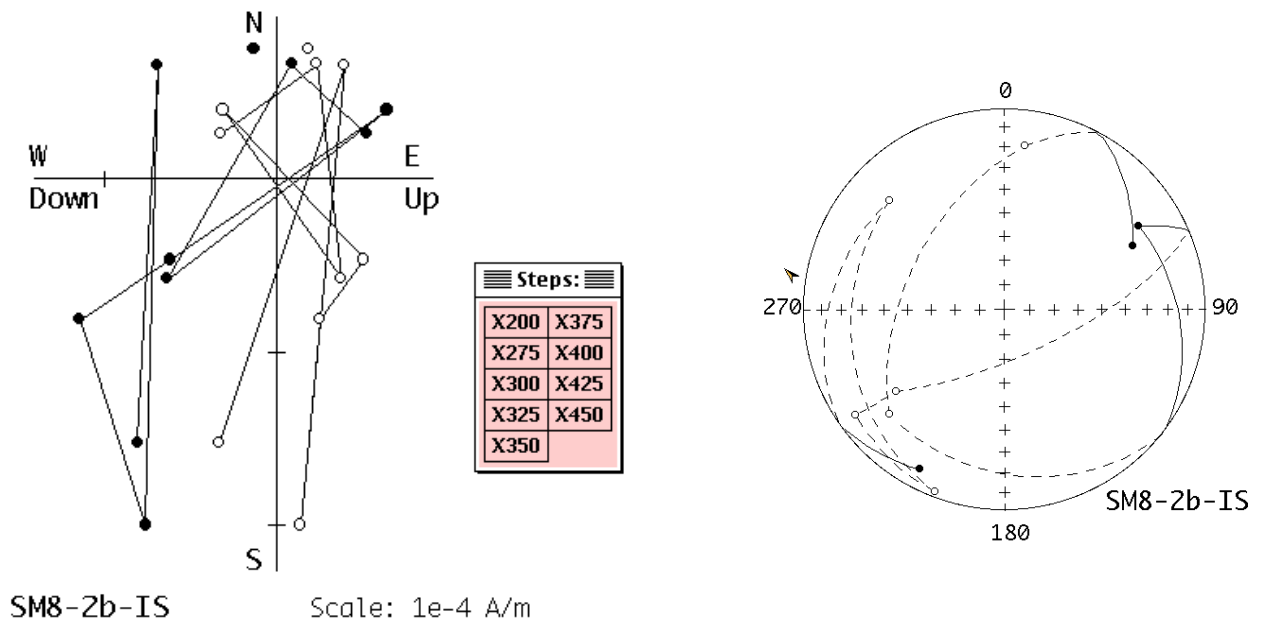**Figure 9:** Thermal demagnetization represented by a chaotic and unusable Zijderveld plot and stereographic projection.
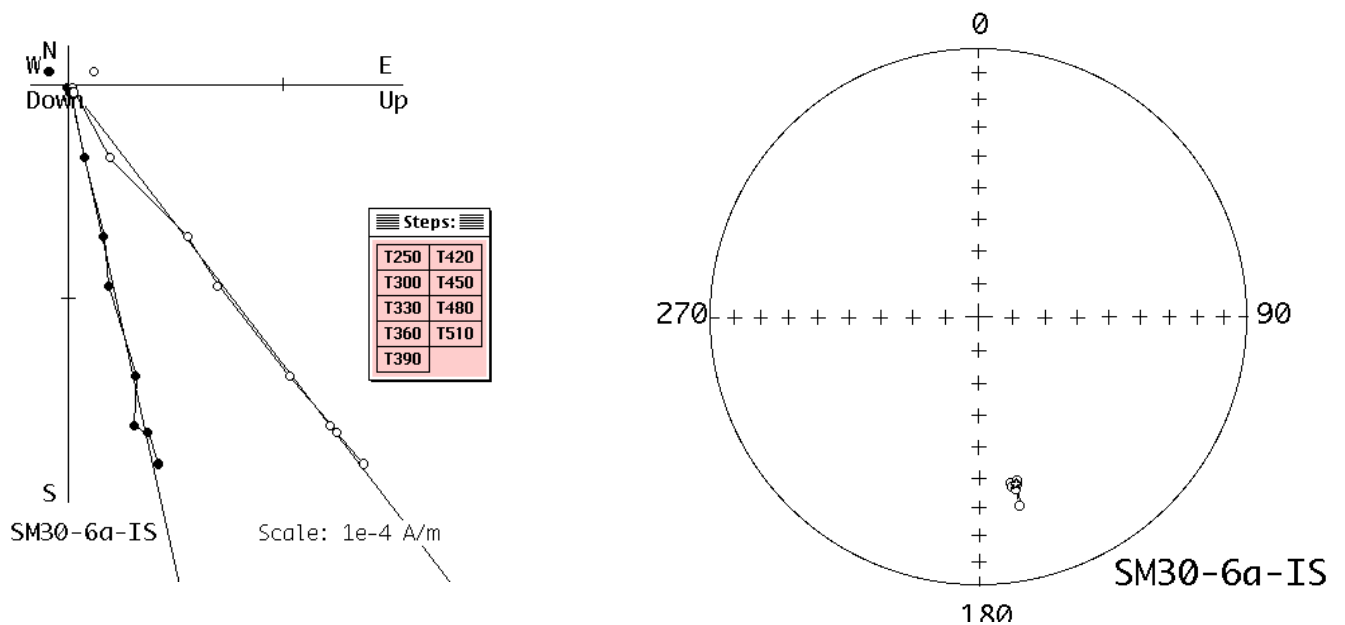
Figure 10: Thermal demagnetization represented by a Zijderveld plot with a clean, uni-vectorial decay of magnetization and a low MAD angle of 1.1° (represented by the best-fit line to the origin on the left), which produces a tightly clustered magnetic direction on the stereographic projection.
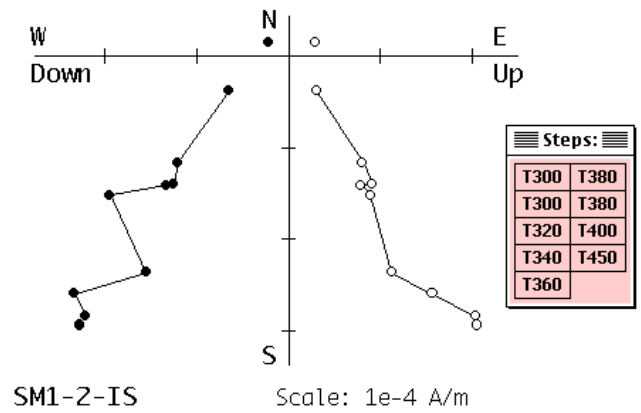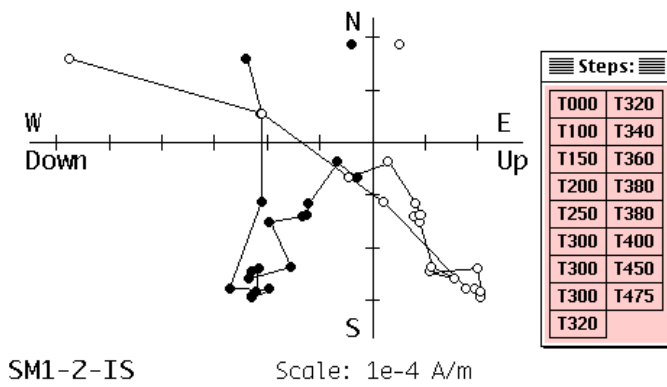
Figure 11: Northerly and downward present day field component is apparent in this sample. This component is removed in order to solely reveal the ChRM in the sample (right Zijderveld plot).
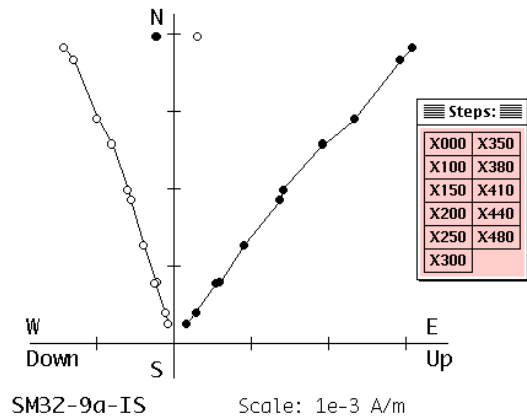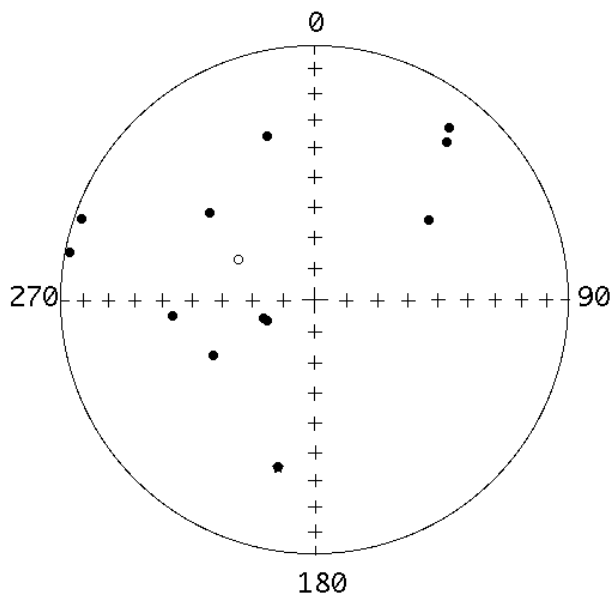
Figure 12: SM32 site represents a highly scattered set of magnetic directions of samples (left). On the top right, SM32-9a is a specimen (within the site 32 mean) that has a quasi uni-vectorial decay and a highly clustered direction (bottom right).
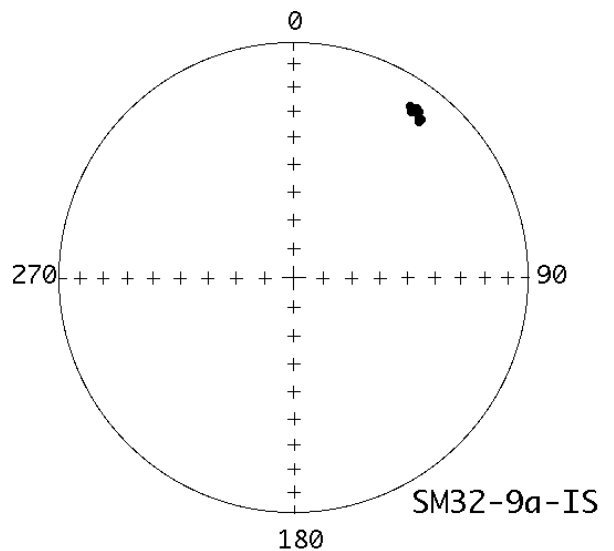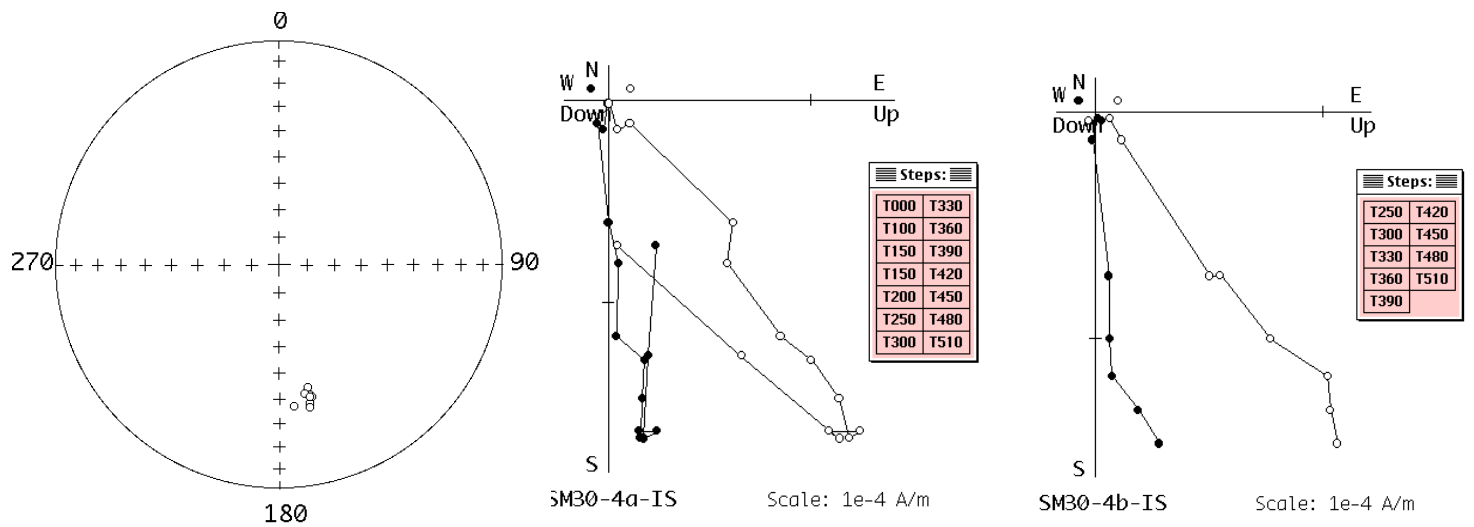
Figure 13: SM30 site mean (left) represents a highly clustered set of magnetic directions of samples with PDF overprints that are removed.
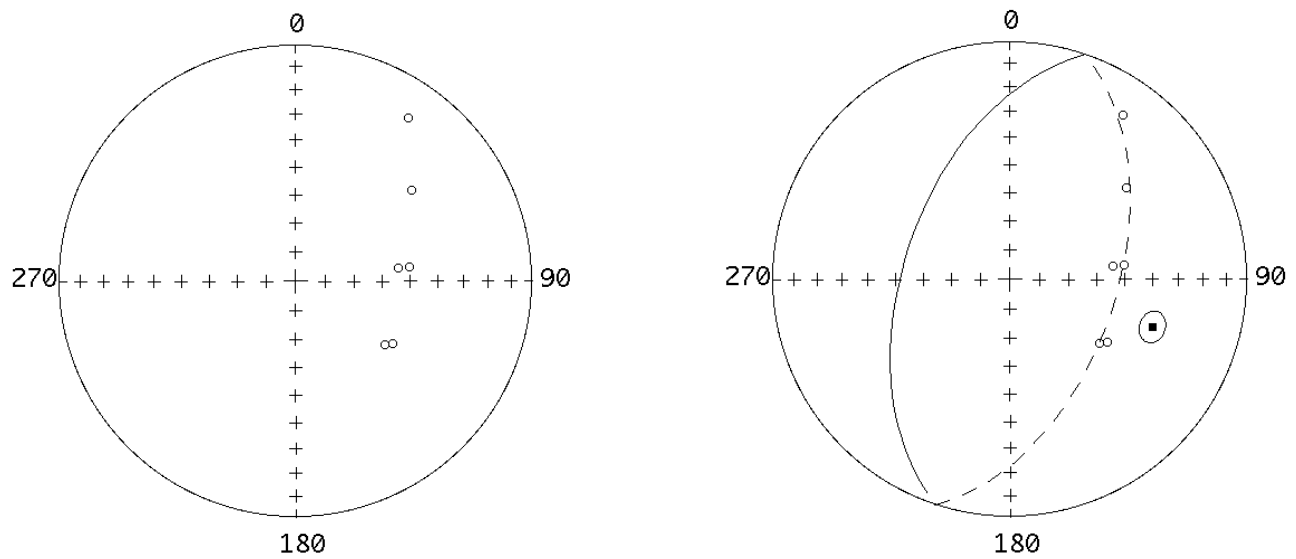
Figure 14: SM2 site directions. Samples fall along a great circle path, which suggests the site mean is somewhere along the plane represented. Square represents the normal to the great circle plane.
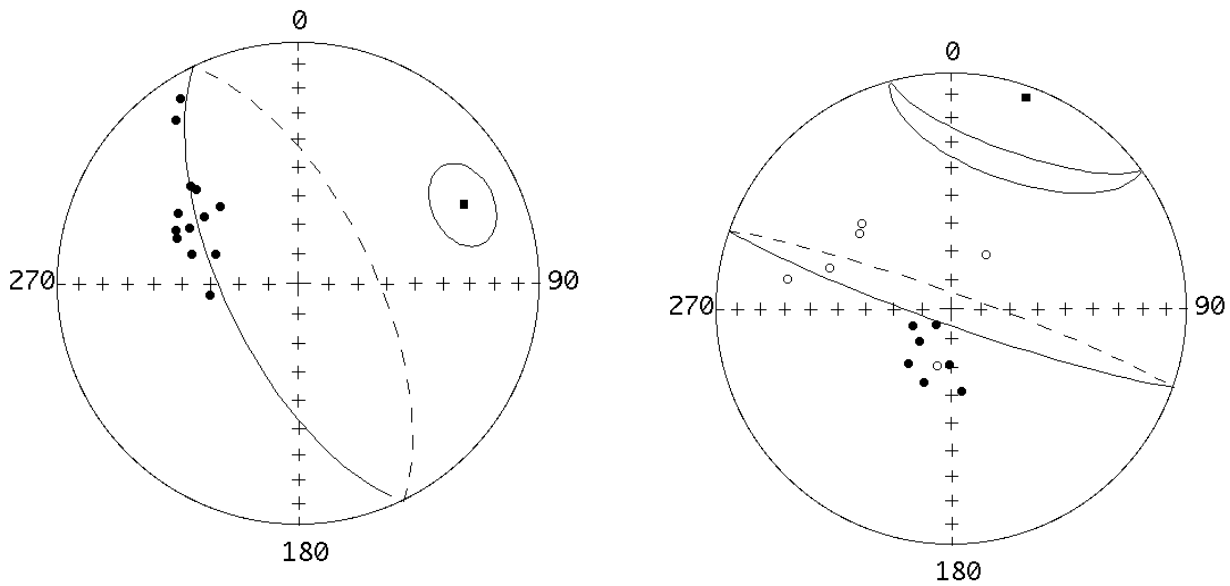
Figure 15: SM31 and SM33 (represented with a great circle) sites. Insitu (left) and tilt-corrected (right).
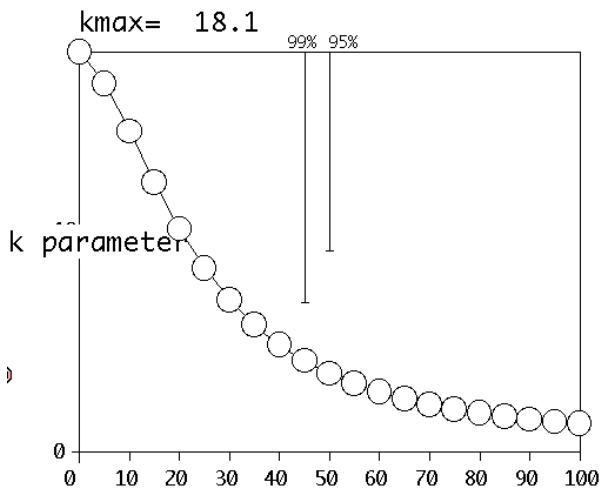
Figure 16: SM31 and SM33 negative fold test. Upon structural correction, the sites become less clustered, indicating magnetization was acquired post-folding. Maximum clustering occurs with normal polarity.
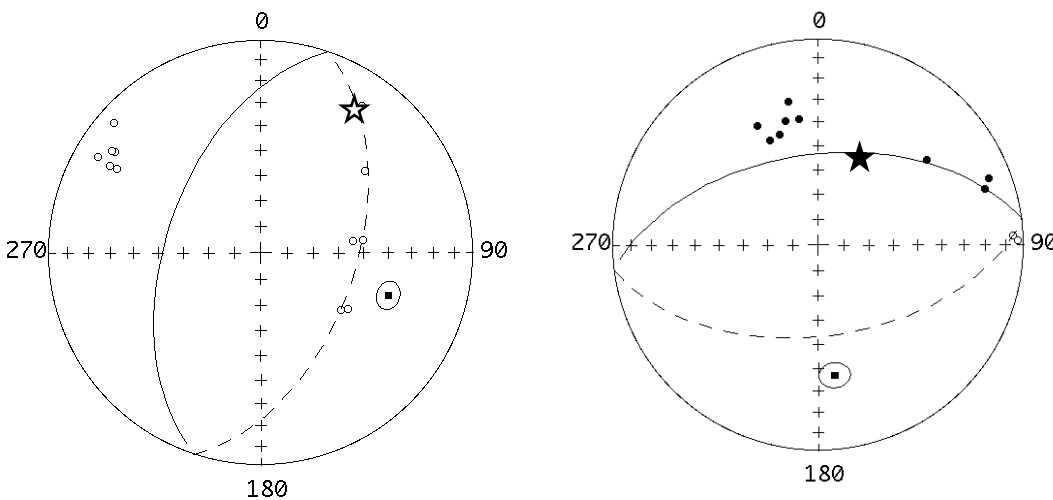
Figure 17: SM2 (represented with a great circle) and SM3 (northerly and upward directions) site insitu (left) and tilt-corrected (right). Star represents the single direction used in fold test.

kmax= 32.2

99% 95%

k parameter
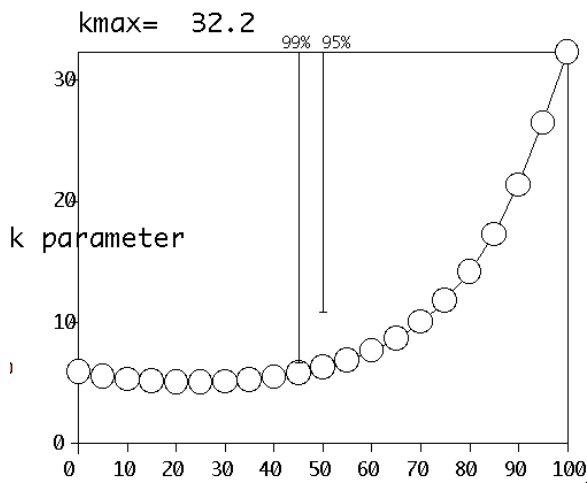
Figure 18: SM2 (made up of one direction) and SM3 fold test that portrays pre-folding magnetization acquisition, as the sites become more clustered upon structural correction.
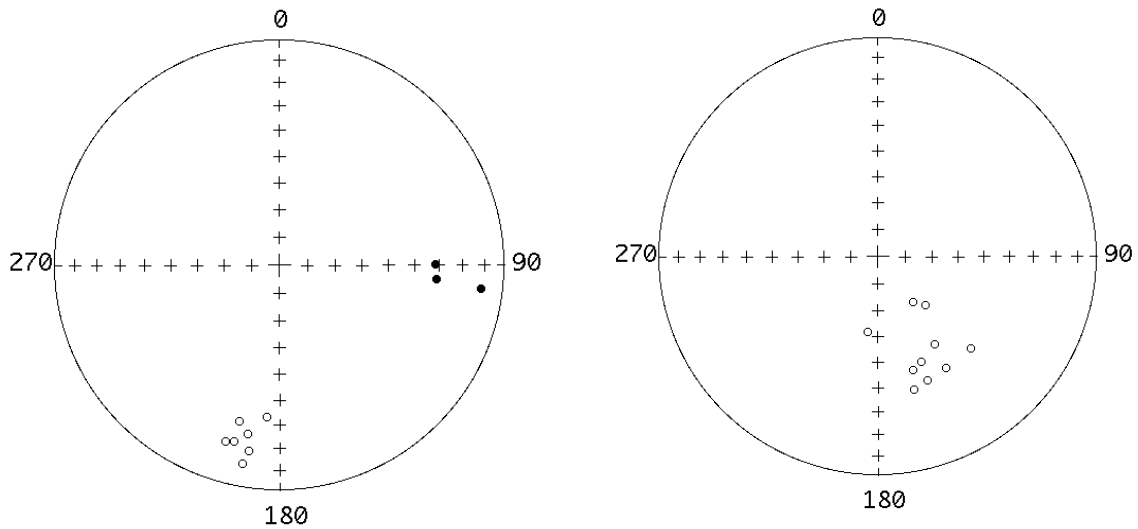
Figure 19: SM4 (southerly and upward directions) and SM7. Insitu (left) and tilt-corrected (right). Maximum clustering occurs with reversed polarity.

kmax= 26.7

99% 95%

parameter
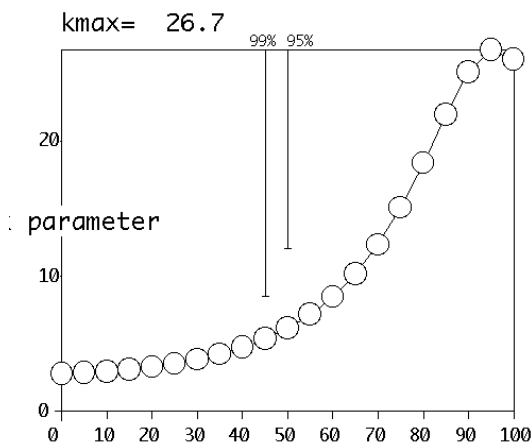
Figure 20: Fold test of SM4 and SM7 that portrays pre-folding magnetization acquisition.
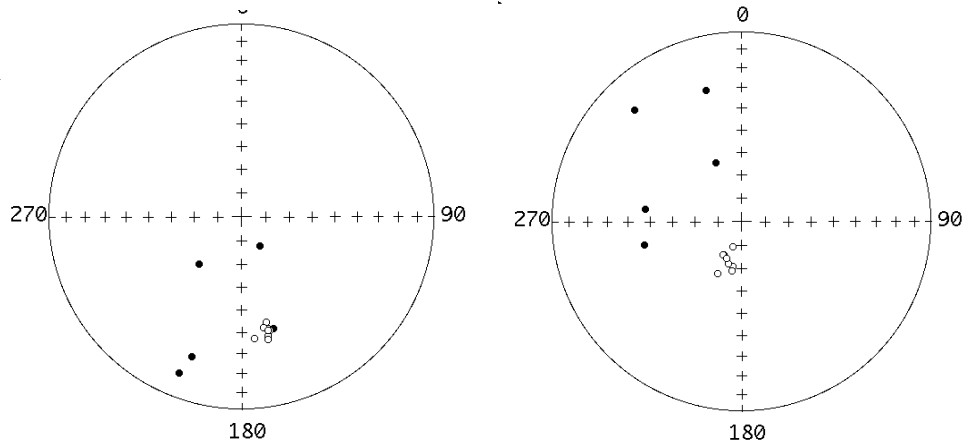
Figure 21: SM18 (southerly and downward directions) and SM30. Insitu (left) and tilt-corrected (right).
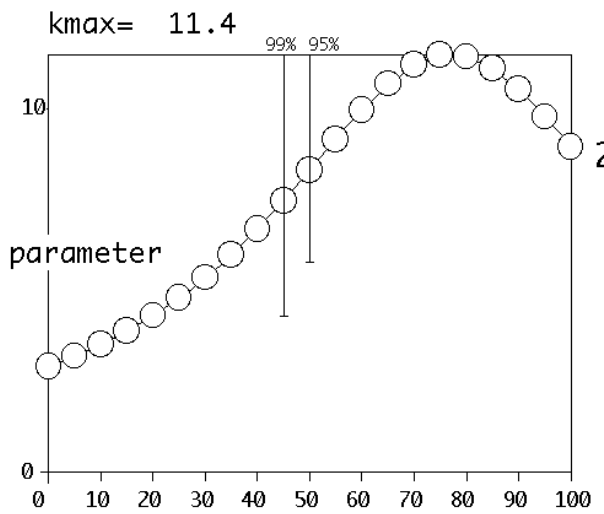
Figure 22: Fold test of SM18 and SM30 that portrays syn-folding. Magnetizations were possibly acquired towards the beginning of the folding event. However, the clustering (i.e., k values) is disappointingly poor.
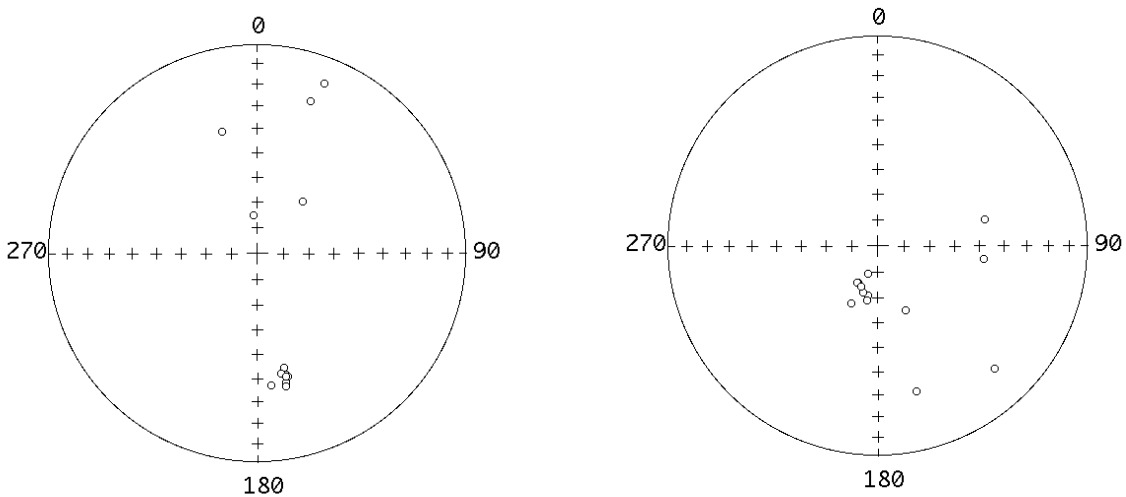
Figure 23: SM18 (northerly and upward directions) and SM30. Insitu (left) and tilt-corrected (right). It is assumed that SM18 has reversed polarity.

Figure 24: SM18 (reversed polarity) and SM30 fold test, which yields a syn-folding result.

kmax= 11.4

99% 95%

‹ parameter
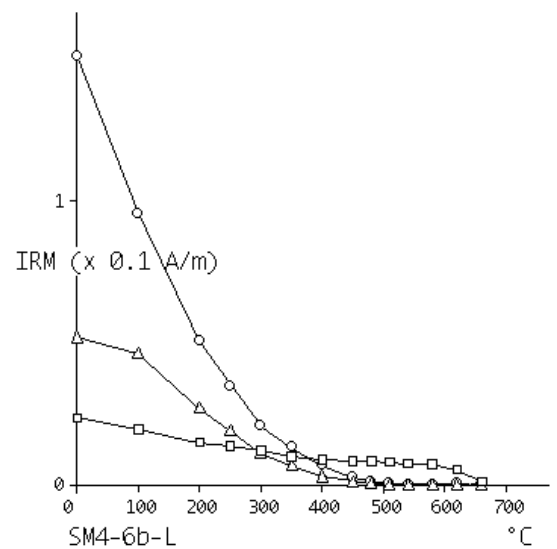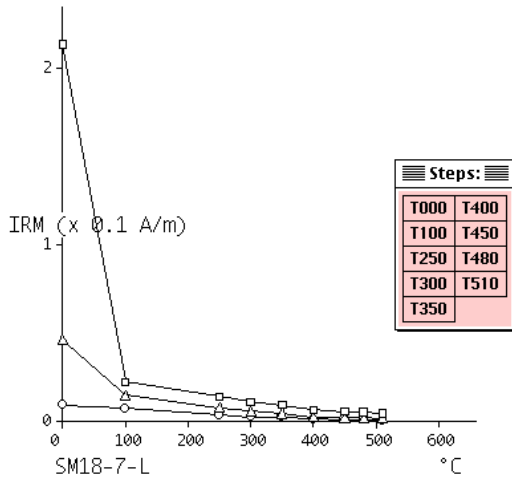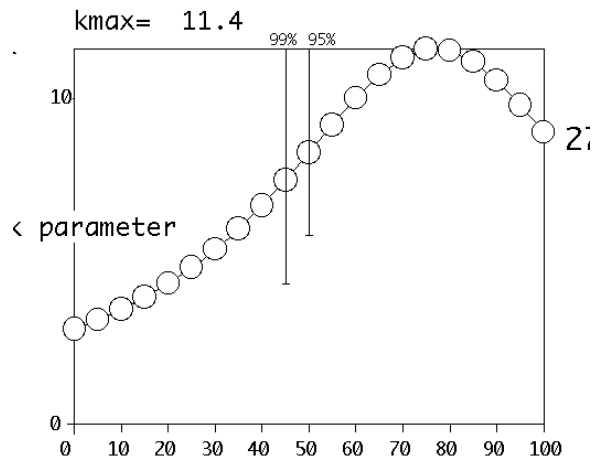
Figure 25 and **26:** IRM curves and decay of magnetizations in two samples. Squares, triangles and circles represent three orthogonal vectors and the coercivities of minerals with the applied magnetizing field (1000mT, 300mT and 120mT respectively). **Figure 25** (left) indicates presence of goethite due to high coercivity and low unblocking temperature. Smooth decay until 560°C indicates magnetite. **Figure 26** (right) decays smoothly to 680°C. Possible presence of laboratory produced CRM owing to oxidation of magnetite to hematite.

≡ Steps: ≡	
T000	T400
T100	T450
T250	T480
T300	T510
T350	

IRM (x 0.1 A/m)

SM18-7-L   °C

IRM (x 0.1 A/m)

SM4-6b-L   °C

Table 1: Site information (see **Figure 1** for locations of sites), organized by site number, number of samples per site, bedding orientation, core information (declination, inclination, statistical parameters), site information (mean declination, mean inclination, statistical parameters). IS: in-situ. TC: bedding structural correction. MAD: Maximum Angular Deviation. *k*: precision parameter. n: number of samples used for data analysis. N: number of samples collected. PDF: present day field direction. D: Downward direction. Data not used for analysis are marked in red and yellow. Sample averages are marked in white.

Site	Sample /Core	n/N	Strike (LHR) dec corr	Dip	Direction	Azimuth dec corr	Plunge (OR2)	Dec IS	Inc IS	Dec TC	Inc TC	MAD	Dec IS	Inc IS	Dec TC	Inc TC	a95	k	PDF
SM1	1	7/8	136	52	SW	96	53	197.8	15.1	194	-30.7	14.1	221.4	-23.7	209.3	-75.2	3.7	271.3	N/NW & D
	2					98	63	220.2	-26.3	201.5	-77.3	6.1							
	3a					107	38	221.1	-23.8	208.3	-75.2	7.6							
	3b					107	38	215.3	-24.9	188.1	-74.1	11.4							
	3avg					107	38	218.2	-24.4	198.2	-74.7	9.5							
	4					85	42	224.3	-24.8	219.1	-76.7	7.4							
	5a					97	18	227.9	-20.3	231.7	-72.2	9.8							
	5b					97	18	225.9	-17.9	225.7	-69.9	11.8							
	5avg					97	18	226.9	-19.1	228.7	-71.1	10.8							
	6					149	51	215.5	-23.7	190.8	-73.2	9.3							
	7					79	60	219.7	-19.7	207.5	-70.9	10.4							
	8					65	52	225	-27.6	221	-79.5	6.6							
SM2	1	6/8	140.4	71.4	SW	80	56	343.9	3.9	324.3	23.5	31.5	108.4	36.9	172.8	36.4	5.2		N & D
	2					105	80	52.2	-37.7	52.2	33.6	17.3							
	4					92	39	34.6	-17.4	26.1	50.8	29.8							
	5					54	72	122.8	-49.5	88.7	-3.2	18.3	GREAT CIRCLE ANALYSIS						
	6					100	55	125.4	-51.7	87.3	-5.6	35.1							
	7a					70	64	70.6	-50.9	63.7	18.3	33							
	7b					70	64	95.8	-56.6	73.6	5.7	40.7							
	7avg					70	64	83.2	-53.8	68.7	12	36.9							
	8					93	80	83.3	-49.9	71.7	15.6	37.3							
	9					54	26	48.2	56.8	232.4	51.7	13.3							
SM3 Inverted	1	6/8	336	126	SW	246	46	304.6	-17.8	332.9	35.5	7.8	303.5	-16.4	335.9	-39.5	5.5	6.6	Incoherent
	2		340	130		242	45	189	-52.8	121.5	47.5	13.1							
	3		340	121		308	49	301	-19	341	43	3.9							
	4		341	129		66	41	262.6	-33	312.2	77.3	7.8							
	5		342	122		32	38	307.1	-16.6	345.5	38	14.1							

SM	#	Frac			Dir														Class
	6		341	120		242	45	302.5	-10.9	351.5	38.6	6.4							
	7		341	120		256	43	311.3	-8.9	348.4	30	7.5							
	8		341	120		316	69	303	-24	335.3	43.6	11.6							
SM4	1	7/7	155	55	SW	66	56	196.8	-19.1	162.6	-44.7	27.7							
	2		151	54		77	27	194.3	-29.2	147.1	-50.4	11.1							
	3		157	60		74	54	190.6	-24.8	148.5	-40.1	8.4							
	4		154	60		85	70	184.7	-32.6	134.8	-40	9.5	191.5	-22.1	153.4	-43	6.1	97.9	N/NW & D
	5		153	57		154	54	190.3	-11.1	164.8	-37.1	8.3							
	6		154	56		42	52	189.1	-17.1	158	-38.6	9.4							
	8		151	56		66	53	194.4	-20.2	157.2	-46.7	6.7							
SM7 inverted	1	3/8	341.5	115.4	SW	131	50	95.2	30.5	142.5	-68.5	37.4							
	2					43	12	96.8	10.6	187	-61.3	33.8							
	3a					81	41	46.6	36.9	15.8	-65.9	36.8							
	3b					81	41	36.6	54.6	39.5	-51.2	26.3							
	3avg					81	41	41.6	45.8	27.7	-58.6	31.6							
	4					231	40	125.7	24.7	150	-41.2	11.2	78.9	32.3	115.9	-78.8	23.5	11.6	N & D
	5					82	44	157.3	-3.4	166.4	-2.3	19.4							
	6					113	61	136.4	0.6	172.2	-22.8	22.7							
	7					73	46	58.8	34.3	23.3	-75.8	20.4							
	8					299	24	89.9	31.2	135.6	-64.3	30							
SM8	1		158.5	67.6	SW	Incoherent													
	2																		
	3																		
	4																		
	5																		
	6																		
	7																		
	8																		
	1		251	75		160	59	147.4	75.4	344.9	29.1	31.6							
	2		250	77		106	46	82.8	-47.8	119.1	-1.2	18.1							

Sample	Sub	Frac			Dir															N&D
SM18	3	5/8	247	80	NW	38	39	201.6	13.6	256.3	46.3	6.8	191.3	45.1	307.8	46.3	32	6.8	N & D
	4		251	82		168	40	221.6	63.2	316.3	20.1	35.8							
	6		251	78		317	36	163.8	39.3	336.3	62.6	16.6							
	8		249	83		159	47	199.5	23.9	277.1	47.7	8.4							
SM30	1	8/8	58	40	SE	316	40	166.5	-40.2	208	-73.7	2.3	167.8	-38.3	199.7	-71.8	2.5	463	N/NW & D
	2		66	38		301	38	166.6	-43.1	198.6	-78.6	1.7							
	3		60	39		314	51	168.5	-40.9	208.7	-73.7	2.7							
	4a		58	36		295	30	174.1	-36.4	204.4	-64.8	3							
	4b		58	36		295	30	173.2	-37	203.8	-65.7	2.9							
	4avg		58	36		295	30	173.7	-36.7	204.1	-65.3	3							
	5a		59	39		304	55	164.3	-38.4	195.4	-73.4	1.9							
	5b		59	39		304	55	168.9	-39.6	207.5	-72.1	2.5							
	5avg		59	39		304	55	166.6	-39	201.5	-72.8	2.2							
	6		62	37		324	49	167.2	-36.6	191.1	-70.4	1.1							
	8		61	37		261	39	167.7	-35	190.8	-68.5	3.3							
	9		57	37		327	49	165.8	-38.8	196.9	-70.8	3							
SM31	1a	7/8	53	54	SE	13	59	284.7	40.1	213.5	59.8	13.4	300	46.6	203.7	71.8	7.1	73	N/NW & D
	1b		53	54		13	59	295.9	51	186.8	65.5	12.6							
	1avg		53	54		13	59	290.3	45.6	200.2	62.7	13							
	2		54	53		340	35	271.2	31.2	225.4	46.5	10.4							
	3		56	49		354	62	293.2	44.1	217.6	65.8	16.2							
	4a		61	48		341	33	308.5	42.3	232.5	73.4	12.2							
	4b		61	48		341	33	315.8	37.2	258.5	77.4	10.9							
	4avg		61	48		341	33	312.2	39.8	245.5	75.4	11.6							
	5a		51	48		52	64	298.3	46.2	208.9	73.2	6.6							
	5b		51	48		52	64	302	38.3	239	75	6.7							
	5avg		51	48		52	64	300.2	42.3	224	74.1	6.7							
	6a		53	47		326	62	313.4	43.9	222	83	6.5							
	6b		53	47		326	62	311.7	43.3	227.2	81.8	6.8							
	6avg		53	47		326	62	312.6	43.6	224.6	82.4	6.7							
	7a		48	53		316	54	286.4	48.4	191.6	64.4	14.9							

Sample	ID	Q			Dir								Notes	
	7b		48	53		316	54	307.1	47.8	171	76.5	12.1		
	7avg		48	53		316	54	296.8	48.1	181.3	70.5	13.5		
	8a		51	51		14	59	293.2	60	171.5	62.7	11.2		
	8b		51	51		14	59	286.4	60.9	173.8	59.4	8.4		
	8avg		51	51		14	59	289.8	60.5	172.7	61.1	9.8		
SM32	1a		243	82	NW								Incoherent	
	1b		243	82										
	2		241	87										
	3a		232	79										
	3b		232	79										
	4		231	65										
	5		243	82										
	6		243	78										
	7		239	79										
	8		239	79										
	9		239	79										
SM33 inverted	1a	6/8	215	100	NW	352	29	322.7	23.8	353.3	-68.2	10.4		Incoherent
	1b					352	29	323.9	9.9	33.6	-71.4	14.7		
	1avg					352	29	323.3	16.9	193.5	-69.8	12.6		
	2					87	25	327.4	10.1	32.9	-67.9	15.7		
	3					331	40	256.7	-27.1	175.3	-30.3	5.2		
	4					8	35	119.3	-34	113.6	65.5	1.1		
	5					38	50	314.6	52.5	313.5	-46.8	17.5	GREAT CIRCLE ANALYSIS	
	6					93	27	285.4	52.3	288.2	-44.8	10.5	64.1 24.7 3.4 21.3 11.8	
	7a					338	30	248.5	59.1	272.7	-25.3	7.4		
	7b					338	30	275.8	60.3	287.7	-35.2	9		
	7avg					338	30	262.2	59.7	280.2	-30.3	8.2		
	8a					42	18	295.6	59.6	298.8	-39.9	21.9		
	8b					42	18	315.3	41.5	319.3	-57.3	28.6		
	8avg					42	18	305.5	50.6	309.1	-48.6	25.3		